

High Frequency Ultrasound Propagation Patterns in Crystalline Silicon

An Honors Paper for the Department of Physics and Astronomy

By Boyang Zhang

Bowdoin College, 2017
©2017 Boyang Zhang

Table of Contents

Acknowledgement	iv
Abstract	v
Chapter 1 Theoretical Introduction.....	1
1.1 Introduction	1
1.2 Elastic Wave Equation	2
1.3 Group Velocity and Slowness Surface	4
1.4 Phonon Focusing Image	7
1.5 Internal Diffraction	8
Chapter 2 Imaging Acoustic Waves	11
2.1 Experiment Setup	11
2.2 Source of Excitation	12
2.3 Transducer Properties	13
Chapter 3. Experiment Data Analysis	15
3.1 Single Line Scan	15
3.2 Ultrasonic Flux Diagram.....	18
3.3 Diffraction Pattern.....	21
Conclusion.....	26
References	27
Appendix.....	28
Color Images in Black and White	28

Acknowledgement

First and foremost, I wish to express my sincere gratitude towards Professor Madeleine Msall, my project advisor. She is incredible and without her this project would not have become a reality.

I would especially like to thank Paul Cheng, who set up the original experiment and guided me through the beginning of the project.

Finally, I would like to thank my family and friends who have offered me support throughout the years and made it possible for me to accomplish this work.

Abstract

This project aims at explaining the propagation of ultrasound through crystalline silicon and experimentally imaging the acoustic waves. Applying the continuum elasticity theory, we can calculate the wave propagation in silicon. Experimentally scanning the energy intensity on the silicon sample surface both along a line and over the entire surface allows us to observe the anisotropic wave propagation in silicon. If the signal is long enough, we can also observe diffraction patterns in energy flux diagrams. Fourier transforming the data enhances the clarity of the diffraction pattern and also allows us to compare the patterns of different frequency components.

Chapter 1 Theoretical Introduction

1.1 Introduction

In order to understand the behaviors of solids, we need to understand the motion of their atoms within the system. A good model for a crystalline solid is a lattice of point masses connected by harmonic springs, as shown in Figure 1.1.

When an external excitation hits the surface of the solid, the point masses vibrate around their equilibrium positions, and subsequently set up a vibrational wave that propagates the energy. The anisotropic elasticity in a crystalline solid causes a directional dependency of ultrasonic wave propagation. Compared to isotropic systems, the propagating wave surfaces in silicon have more complicated features, as shown in Figure 1.2 [3]. An important phenomenon in anisotropic crystals is that the phase velocity, which describes the direction and speed of the wave's phase front, does not describe the rate of energy travel, as I will show in greater details in the following sections.

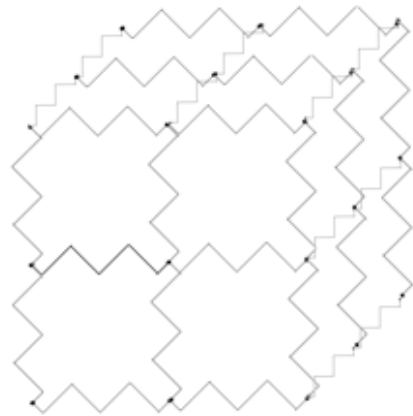


Figure 1.1 A lattice of point masses connected by harmonic

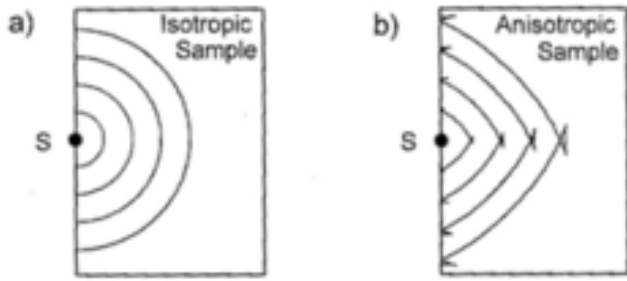


Figure 1.2 Wave emanating from a point source in a) an isotropic medium, compared to b) in an anisotropic medium [3].

1.2 Elastic Wave Equation

Following the methods in J.P. Wolfe's book *Imaging Phonons*, I present the mathematical basics of wave propagation in crystalline solids, using continuum elasticity theory. For a single point mass and harmonic spring, Hooke's law provides a relation between spring constant, force and displacement from equilibrium. Similarly, for a lattice modeled as multiple point masses connected by harmonic springs, the generalized Hooke's law relates the stress and strain through the elasticity tensor. The elasticity in this model is a rank-4 tensor. Both the strain and stress tensors are rank two. Stress measures force per unit area, or pressure. It is represented in component form as:

$$\sigma_{ij} = F_i/A_j$$

The strain tensor measures how the lattice distorts from its equilibrium in response to applied stresses. It is represented in component form as:

$$\varepsilon_{lm} = \partial u_l / \partial x_m$$

where u_l is the displacement from equilibrium.

Waves in solids usually consist of longitudinal waves and transverse waves or their combination. Longitudinal waves have stress tensor in form σ_{ii} . This wave induces a compressive stress in which the net force is normal to the surface perpendicular to the

wave's propagation direction. For transverse waves, the stress tensor has indices that are different from each other, σ_{ij} ($i \neq j$). This wave induces a shear force that has direction parallel to the surface perpendicular to the wave's propagation direction.

The stress and strain tensors are related by the general Hooke's law.

$$\sigma = C : \varepsilon$$

where ":" indicates a sum of two of the four indices in C. The elasticity tensor C contains elasticity constants that depend on the spring constants of the medium. C also has unit of pressure, which matches the unit of stress, since the strain is dimensionless. In component form we can write this as:

$$\sigma_{ij} = C_{ijlm} \varepsilon_{lm}^1$$

Notice that the expression above is equivalent to nine equations, as the two indices in σ each can have value x, y, z, and elasticity tensor has 81 components (a 3x3x3x3 rank-4 tensor). Fortunately, the symmetry of σ 's and ε 's indices and the symmetry of cubic crystal reduces the elasticity tensor to only 3 independent components.

Substituting σ_{ij} using the relation mentioned above, we have the elastic wave equation:

$$\rho \frac{\partial^2 u_i}{\partial t^2} = C_{ijlm} \frac{\partial^2 u_l}{\partial x_j \partial x_m}$$

This is the equivalent of Hooke's law in 3 dimension. On the LHS we have the equivalence to mass x acceleration, where ρ is the density of the solid and second

¹ This equation uses Einstein summation notation: Repeated indices on the same side of the equation indicates a summation. E.g. $A_i * B_i = A_1 B_1 + A_2 B_2$, where $i = 1, 2$

derivative of the displacement in i-direction with respect to time. On the RHS we have the elasticity constant contracted with the spatial second derivative.

To solve this equation, we assume a plane-wave solution:

$$\vec{u} = u_0 \vec{e} e^{i(\vec{k} \cdot \vec{r} - \omega t)}$$

where \vec{k} is given, and we will determine frequency ω and unit polarization \vec{e} .

Apply the solution back to the elastic wave equation above,

$$\rho \omega^2 e_i = C_{ijlm} k_j k_m e_l$$

we can rewrite this as an eigenfunction with eigenvalues $\nu = \omega/k$ and eigenvectors \vec{e} , if

we define the wave normal $\vec{n} = \frac{\vec{k}}{|\vec{k}|}$:

$$(\frac{C_{ijlm} n_j n_m}{\rho} - \nu^2 \delta_{il}) e_l = 0$$

This is the generalized classical wave equation in an anisotropic medium and also known as the Christoffel equation. The three eigenvalues of the function for the three spatial components are three modes of phase velocity with unit polarization \vec{e} for a given \vec{k} .

The three modes are normally labeled as longitudinal, fast transverse, and slow transverse. An important clarification for these modes is that a longitudinal mode does not generally have purely longitudinal polarization. They are usually a mixture with one polarization present in greater proportion.

1.3 Group Velocity and Slowness Surface

Once we obtain the phase velocities of the solid with elasticity C, we can construct the slowness vector $\vec{s} = \vec{k}/\omega(\vec{k})$ to visualize the result. The slowness vector has direction along \vec{k} and magnitude $1/\nu$. If we plot out the slowness vector in all \vec{k} -

directions, we have a 3-D slowness surface which represents a set of equal frequency k-space points. If we take a slice of the surface at a given angle, we can construct a 2-D slowness surface. Figure 1.3(a) shows the calculated slowness surface in the (100) plane of silicon. From the outside to the inside, the three layers of slowness surface correspond respectively to slow-transverse, fast-transverse and longitudinal mode. The slowness surface for a given mode is a constant-frequency in k-space. The gradient of slowness with respect to \vec{k} , (i.e. vectors normal to the slowness surface) is the group velocity:

$$\vec{V} = \nabla_k \omega$$

Group velocities describe the propagation of wave-packets. The excitation of the sample surface generates oscillations which are combinations of waves with multiple different wavelengths. Group velocity also describes the propagation of energy in solids, since energy travels with the wave-packet, instead of with a component wave of a particular frequency.

If we calculate the group velocity using the slowness vectors in the slowness surface in Figure 1.3(a), we can obtain the group velocity cross-section corresponding to the same (100) plane in silicon, shown in Figure 1.3(b). The cross-section shows constant-time surfaces for a single mode in real space. It is equivalent to the wave front of a point disturbance spreading energy in the solid. The particularly interesting shape of the slow-transverse group velocity surface is the direct result of inflections on the slowness surface. For example, in Figure 1.3 (a), the three vectors normal to the slow-transverse slowness surface, highlighted in orange, correspond to three group velocity

$\vec{v}_1, \vec{v}_2, \vec{v}_3$ that have same direction \vec{V}_g but different speeds. As a result, in the group velocity surface Figure 1.3 (b), we see that there are three data points along the \vec{V}_g direction. Since many vectors normal to the slowness surface around the inflection point are nearly parallel to each other, there will be a concentration of group velocity in those directions. The data point density on the group velocity surface in Figure 1.3(b) represents the amount of wave energy in a given direction, so we can expect to see higher energy intensity in the region close to the axis. For the longitudinal mode, the slowness surface has a near circular cross-section, which indicates a much weaker directional dependency for group velocities.

Another interesting feature of the two surfaces is that, for slowness surface in Figure 1.3(a), different modes' surfaces can touch each other but will never crossover, by definition. Thus, the slow-transverse mode is always slower than the fast-transverse mode in a given k-direction. However, slow-transverse mode's group velocity in a given direction in real space can actually be faster than the fast-transverse in the same direction, which is shown in Figure 1.3(b) around the group velocities corresponding to the inflection points on slowness surface.

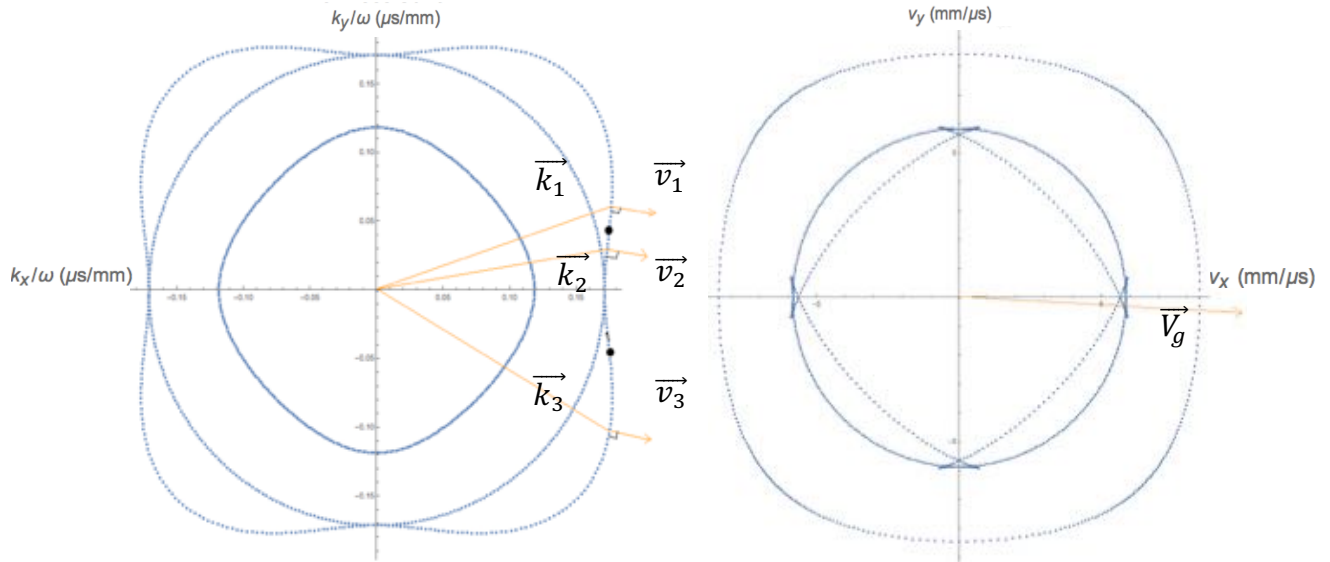


Figure 1.3 (a) Calculated slowness surface in the (100) plane of silicon

Figure 1.3 (b) Calculated group velocity cross-section in the (100) plane of silicon

1.4 Phonon Focusing Image

If we calculate the group velocity from the entire 3-D slowness surface, we can calculate the travel time for the wave energy arriving at any planar surface at a fixed distance from the excitation point. In simpler terms, we can create a density map of the energy flux. Since group velocity describes how energy travels in the solid, this density map depicts the distribution of energy, which is called the phonon focusing pattern.

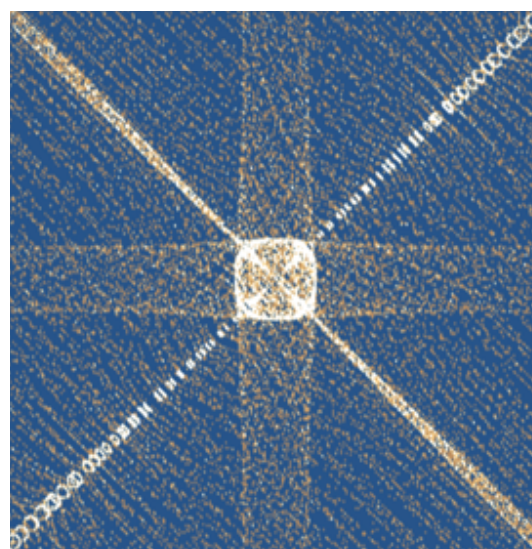


Figure 1.4 Calculated Phonon Focusing Image

Figure 1.4 shows the phonon focusing image on the X-Y plane, 9.8 mm away from the point excitation at the center of the surface in z-axis direction. Regions with higher intensity along the diagonal directions are due to the fast transverse mode. These are called FT ridges. The horizontal and vertical high-intensity bands are called ST ramps. They are results of the concentration of group velocities in directions with a small angle from the axis mentioned in last section. These high intensity features meet at the center of the image create a square region of high energy flux. For the point-like excitation, we expect the center to be circular for an isotropic medium, but the inflection on slowness surfaces for anisotropic medium causes these non-circular of energy concentrations.

1.5 Internal Diffraction

Our calculated phonon focusing image assumes that the propagating waves cannot interfere with one another. If the excitation creates wave pulses that last for longer times, multiple waves may arrive at the detection surface simultaneously and interfere with one another. In this case the image will deviate from the expected ultrasonic flux pattern in the experiment. The feature that is missing in the calculated image is the diffraction pattern. Figure 1.5 shows part of the slow-transverse group-velocity cross-section from figure 1.3(b). If we consider a

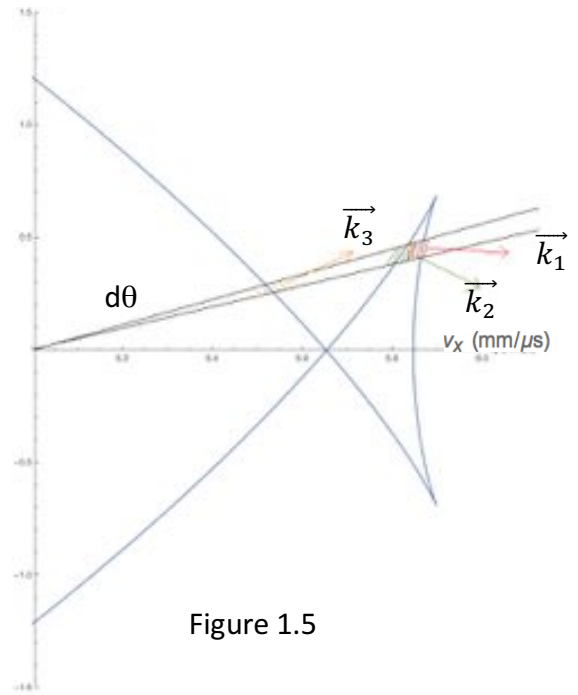


Figure 1.5

small angle $d\theta$ and assume it is small enough that all group velocities within travel along the same direction, we can see that there are three group-velocities corresponding to three different \vec{k} -vectors. Since we can interpret the group velocity surface as the propagating wavefront, when the excitation source is long, for example a tone burst signal, there are multiple wavefronts of the same shape in the region. In Figure 1.5, segments of the multiple wavefronts within the $d\theta$ region are shown. A later oscillation's \vec{k}_1 can interfere with an earlier oscillation's \vec{k}_2 . They will destructively interfere with each other if they have a phase difference of π . Then, on the detection surface correspond to the angle $d\theta$ will show a intensity minimum.

For modest length tone burst signal, only interference between \vec{k}_1 and \vec{k}_2 is visible. If the slowness surface around the inflection is perfectly flat, then the two k vectors will always constructively interfere. However, in reality there is curvature in this region. If we look at the superposition of two waves with \vec{k}_1 and \vec{k}_2 , we have:

$$e^{i\vec{k}_1 \cdot \vec{r}} + e^{i\vec{k}_2 \cdot \vec{r}} = 2\cos\left(\frac{\vec{k}_2 - \vec{k}_1}{2} \cdot \vec{r}\right) * e^{i\frac{\vec{k}_1 + \vec{k}_2}{2} \cdot \vec{r}}$$

\vec{r} is the displacement vector measured from the excitation point. We want $\frac{\vec{k}_2 - \vec{k}_1}{2} \cdot \vec{r} = \pi/2$ to find the intensity minimum. The angle between the maximum intensity (at the inflection) and the first minimum is:

$$\Delta\theta \approx \frac{|\vec{V}_1 - \vec{V}_0|}{|\vec{V}_0|} \propto \left(\frac{\lambda}{r}\right)^{\frac{2}{3}}$$

Where \vec{V}_1 is the group velocity at first intensity minimum, and \vec{V}_0 is the group velocity at the maximum. The angle's correlation with wavelength and displacement indicates that

a thicker sample or a higher frequency both contribute to a finer diffraction pattern. In Hauser and Wolfe's research, this phenomenon is called "Internal Diffraction" [2]. A simulation of the diffraction pattern requires a significant amount of computing time. Various research groups have studied the rigorous mathematical simulations, see Figures 1.6, 1.7. The simulation results are cited as reference for comparing with experiment data in section 3.3.

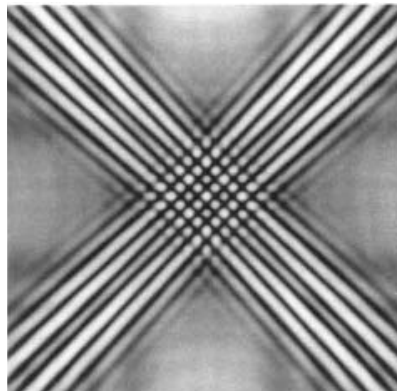


Figure 1.6 Theoretical ultrasound image of a 2-cm cube of silicon at 15 MHz, covering a scan range of 1.5cm*1.5cm [2] (This sample image is rotated by 45 degrees compared to my data images)

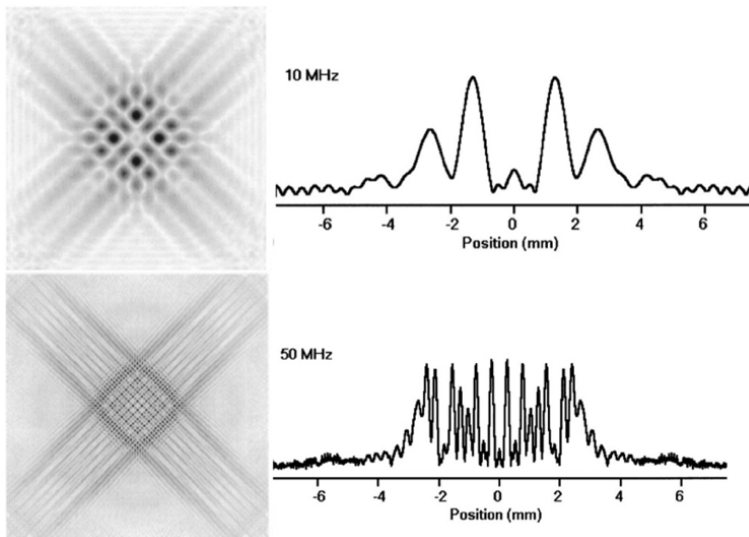


Figure 1.7
On the left: Calculated amplitude image of an (001)-oriented 20mm thick silicon crystal, at f=10 and 50 MHz
On the right: Amplitude variation along the center line
Notice that higher frequency leads to finer diffraction patterns [4].

Chapter 2 Imaging Acoustic Waves

2.1 Experiment Setup

The schematic diagram of our acoustic wave propagation imaging apparatus is shown below in Figure 2.1.

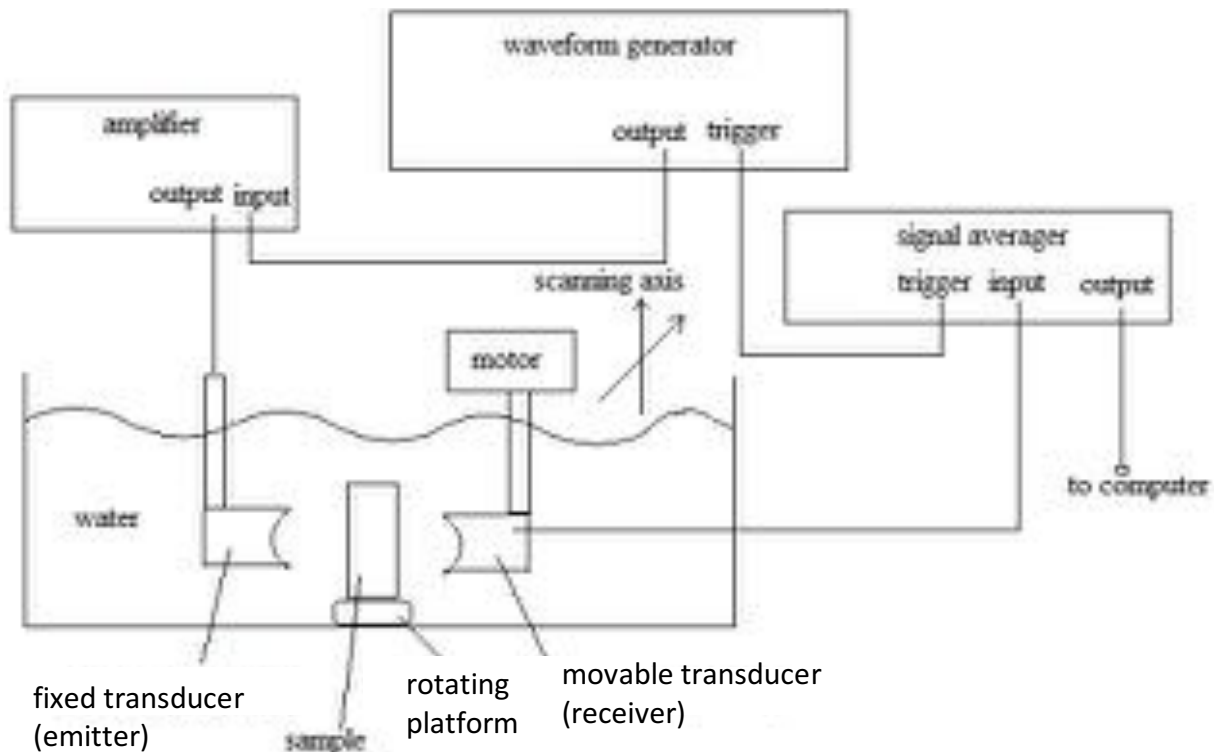
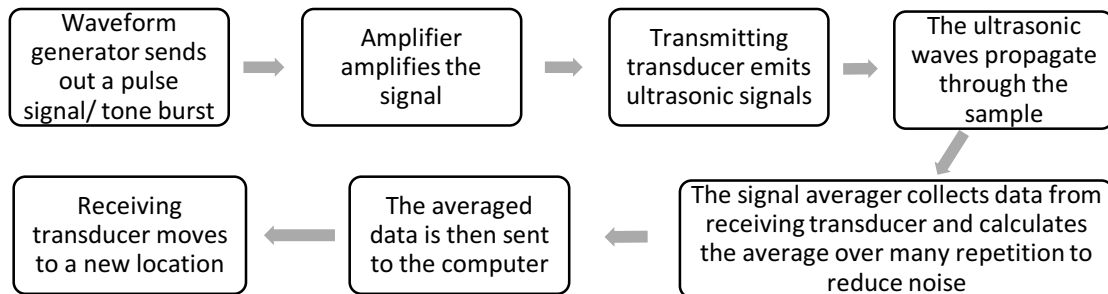


Figure 2.1 Schematic Diagram of the Experiment Setup

The flow diagram shows the typical process of recording data. The waveform generator creates a signal, which is then amplified. The first transducer receives the amplified signal and transmits it as sound waves through the sample under water. On the other side of the sample, another transducer receives the signal. The signal averager collects data from the receiving transducer, and records the average of a given number of samples to reduce noise. The data is then sent to the computer for storage. Finally,

after the data is stored, the computer may also issue commands to move the receiving transducer to a new position or to change the rotation of the sample.



2.2 Source of Excitation

We use the Model 395 100MHz arbitrary waveform generator from Wavetek as the source of excitation. This waveform generator allows us to control the transmitting signal's shape, frequency, and pulse length.

There are two kinds of signals used for the experiment, pulse signal and tone burst signal, shown in Figure 2.2. The waveform generator's standard sine-wave function can generate both kinds of signals by limiting the number of wave cycles at a given frequency. However, there is a 10MHz frequency limit when the generator controls the pulse length. For our experiment, most data are taken at 9 MHz or below.

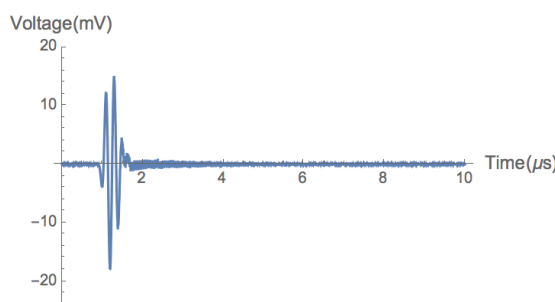


Figure 2.2(a) 5MHz Pulse Signal

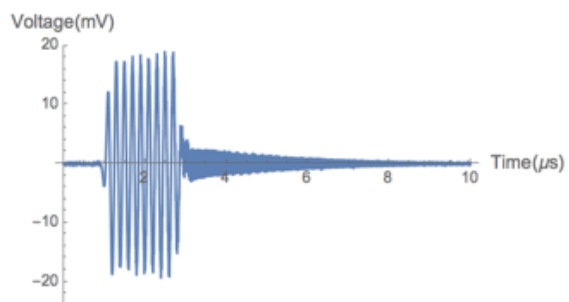


Figure 2.2(b) 5MHz Tone Burst Signal

Figure 2.3 shows the Fourier transforms of 5MHz signals of different duration. While all three signals of different duration have prominent frequency at 5MHz, the longer pulse has higher power and narrower bandwidth, because of more cycles at the set frequency. In Figure 2.2(b), we can see that the longer signal also has a longer ring down. The tone burst signal carries more energy and therefore requires longer time for the waveform generator to cut off the signal. This is reflected in the Fourier transform as small peaks of frequencies around the prominent frequency.

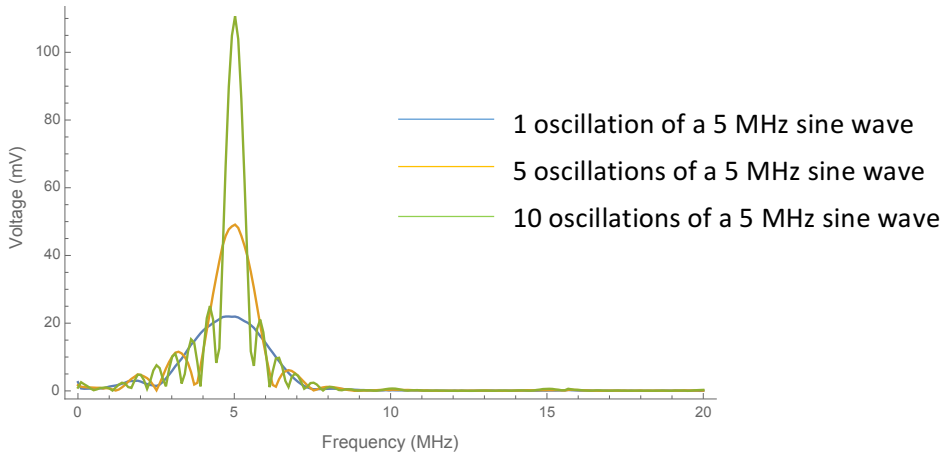


Figure 2.3 Fourier Transforms of Signals of Different Length

2.3 Transducer Properties

In the experiments we use Panametrics V315 10 MHz spherical transducers. These transducers transmit or receive plane waves from a spherical surface that converges emitted waves at focal spot. The focal distance surprisingly does not largely influence the excitation pulse, as long as the transducers are in the broad range of focal distance. The reason for this insensitivity of focal distance is discussed in Hauser's thesis. If the transducers are too close together or too far apart, the signal will focus within the sample or before reaching the sample. However, the signal will be refracted at the

sample surface with angles depending on the incident wavevector direction, and the focal region becomes distorted [3].

By measuring the signal strength as a function of distance, we find that the focal spot size is around 0.5mm and it remains unchanged in the broad range of focal distance. When we measured the power difference of the receiving signal at different distances, the data also shows the insensitivity of focal position, as seen in Figure 2.4. Although the power ratio between transmitting and receiving signal is related to the distance between transducers, the difference is negligible (around 0.2% power difference over 1 cm). However, for the sake of accuracy, the transducers are set at the nominal focal distance when recording data (2.1cm from transducers to sample surface). This is easily achieved by maximizing the reflection signal.

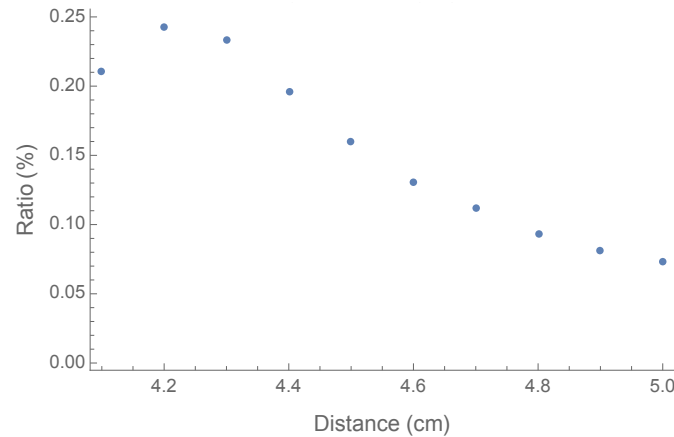


Figure 2.4 Power Ratio of Receiving to Transmitting Signal
vs. Distances between Transducers

Chapter 3. Experiment Data Analysis

3.1 Single Line Scan

If we scan across a line on the sample surface and record the signal intensity over a period time, we can directly observe the wavefront of energy propagation in the direction defined by the excitation point to the scan point. Figure 3.1(a) and (b) shows two different single line scans over the same 8mm along x-scan direction. Both scans use 9MHz pulse signals with a 20mm x 20mm x 9.8mm silicon sample. We define the 20mm x 20mm sample surface the receiving transducer is scanning as the x-y plane. Figure 3.1 (a) shows the energy arrival along the 8mm line in x-direction at the height as the excitation on the other side of the sample. 3.1 (b) shows the energy arrival along 8mm line in x-direction one sample thickness higher from the excitation on the other side of the sample, i.e. $y = 9.8\text{mm}$.

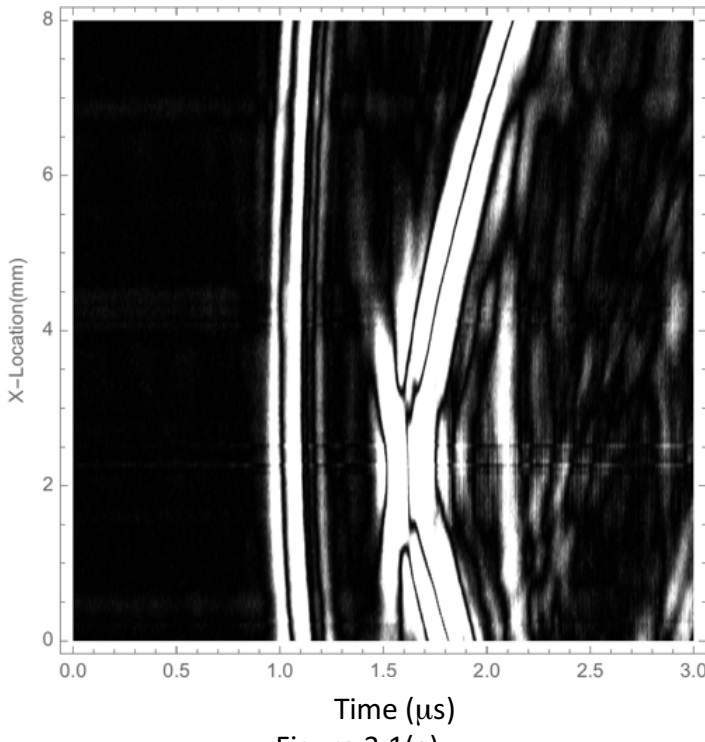


Figure 3.1(a)

Figure 3.1 (a) and (b) are contour plots of energy intensity. They show the energy intensity at a given x-location and time t . Bright regions in the graph indicate high energy intensity.

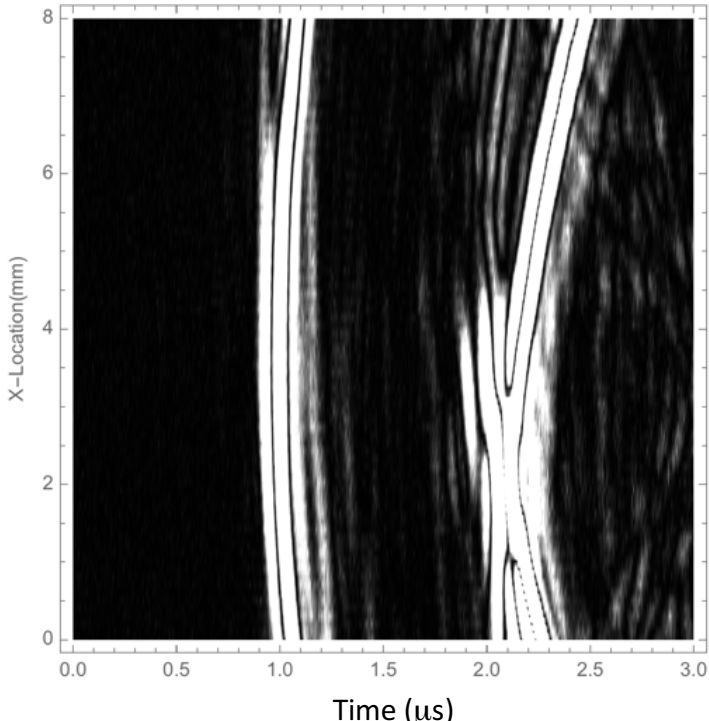


Figure 3.1(b)

- (a) The scan line is at the same height as the excitation ($y = 0$)
- (b) The scan line is 9.8mm higher than the excitation ($y = 9.8$)

Both graphs show wavefronts corresponding to the longitudinal and slow-transverse mode, and they agree with the group velocity simulation in chapter 2. The longitudinal mode has higher speed and therefore arrives earlier. The transverse mode is slower and therefore arrives later with a wider spread in arrival time. The transverse mode shows the folding wavefront due to the anisotropic elastic response of the solid. The difference Figure 3.1 (a) and (b) demonstrates the directional dependency of group velocities. In 3.1(b) the arrival time difference between the two modes is larger than in 3.1(a) because of both different speed and distance. If we compare the same mode in two graphs, we can again see the directional dependency. The longitudinal mode speed remains relatively unchanged in the two graphs. The transverse mode, on the other hand, has a higher speed in 3.1(b), since the arrival time has a smaller spread even with longer travel distance compared to 3.1(a).

Single line scans can also provide interesting information about the reflected signals. If we record the data with longer time frame, we are able to see the signals that have been bounced off the sample surface twice or four times (i.e. travels through the sample 3 times or 5 times before detection). Figure 3.2 shows the X-t plane at $y = 9.8\text{mm}$. In the graph, if we eliminate the signal travel time in water, $t = 0$ corresponds to the time when the ultrasonic wave first hits the sample surface. Setting this time as zero is helpful for finding reflection signals. Previous researchers have shown that when the wave bounces off the sample surface, it can change modes [1], as shown in Figure 3.3. Each wavefront arrival in Figure 3.3 is labeled with the number of laps taken at each speed. $3L$, for example is a wave that has traveled through the crystal 3 times at the L speed. $2LT$ has traveled twice at the L speed and once at T , etc. Similarly, in my experimental data (Figure 3.2) I have marked the $3L$ mode (travels through the sample 3 times in longitudinal mode) at around $3\mu\text{s}$, the $2LT$ mode after it and even the $3T$ mode before the $6\mu\text{s}$ mark. Later reflections are not very clear in the experiment image. The size of the silicon sample relatively small compared to our scan range. As a result, the wave can also bounce off the side of the sample which creates unwanted noise at later times.

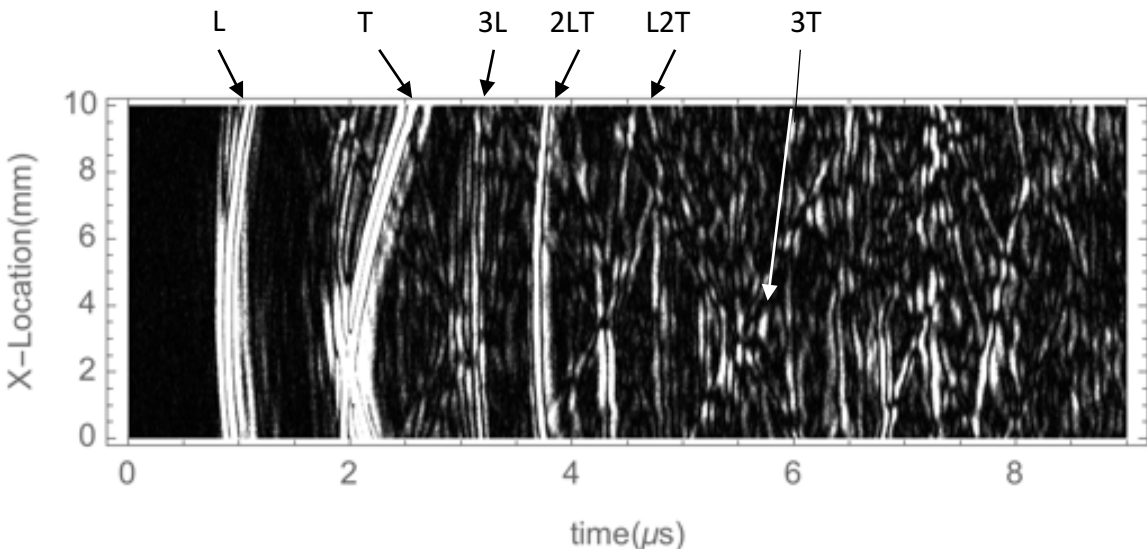


Figure 3.2 Contour plot of energy intensity on the x-t plane at $y = 9.8\text{mm}$, scanning 10 mm in x direction and a total of $9\mu\text{s}$. Brighter regions indicate higher intensity

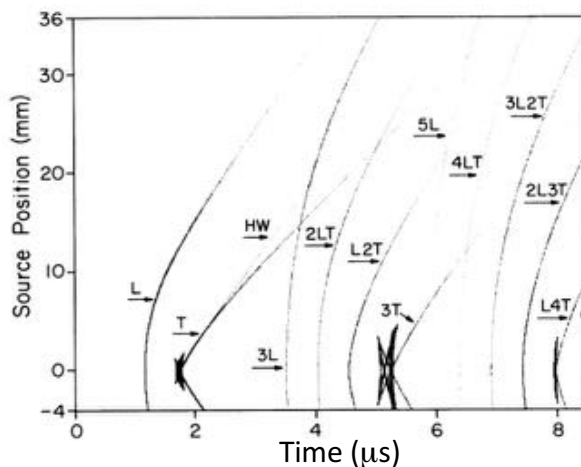


Figure 3.3 Calculated scan image corresponding to 8 mm off epicenter of a [100]-oriented disk-shaped silicon single crystal of thickness 9.91 mm
[1]

3.2 Ultrasonic Flux Diagram

Instead of scanning along one direction, we can make multiple single line scans in both x and y directions. Then we will obtain a “data cube”, with information about the intensity at a given x, y location and time t. Integrating the data over time, we will have a 2-D intensity map on the sample surface. Using the same 9MHz pulse signal, Figure 3.4 shows the energy distribution on the silicon sample surface in a $10\text{mm} \times 10\text{mm}$ region. The recorded signal length is $3\mu\text{s}$, starting at the $t = 0$ set previously in single line scan.

Because of the symmetry in cubic crystal, we only need to scan part of the sample surface. This figure shows features that agree with our phonon focusing image in figure 1.4 with slight deviation. We can clearly see the high intensity bands caused by the slow-transverse mode. The difference in intensity between the two bands is a result of the imperfect cut of the sample, that the sample is slightly thicker on top (large x-value). In the phonon focusing image we also see higher density along diagonal axis, but in our experiment image, the feature is not as pronounced and shows only when close to the center. The reason behind this deviation is that the focused acoustic beam couples very weakly with the FT mode. (Wolfe 1998)

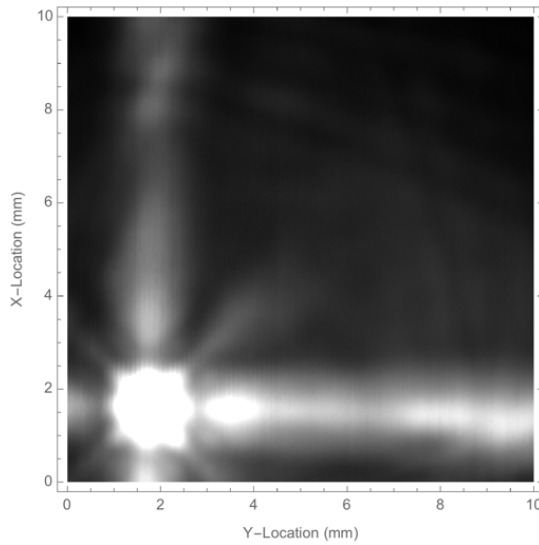


Figure 3.4 Flux diagram
on 9.8mm thick silicon
sample surface from 9
MHz pulse signal

Instead of integrating the signal over the recording time interval, we can also look at the energy intensity on the sample surface at a particular time. This allows us to observe the anisotropy of the sample for another perspective. The series of figures in 3.5 show the arrival of the transverse mode on the scanning surface. For a point-like excitation, if the energy travels isotropically, we would expect to see a circular signal on the sample surface. However, here the transverse mode's arrival time and intensity

shows the effect of folding wavefronts in group velocity cross-section. The signal is non-circular with concentration of energy in the x and y direction. The later time graphs are good examples showing transverse mode have higher intensity and speed along the x-y axis across the center, as signals in such directions arrive at the same time as other signals that have traveled less distances. The slight distortion seen in (c) and (d) is a result of an error of the scanning controls that do not always move properly in the y-direction.

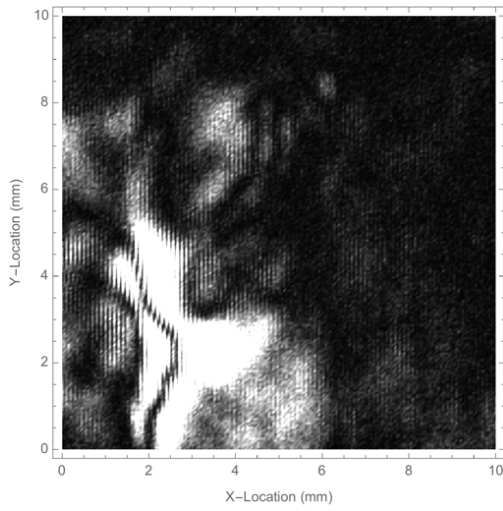


Figure 3.5 (a) $t = 1 \mu\text{s}$

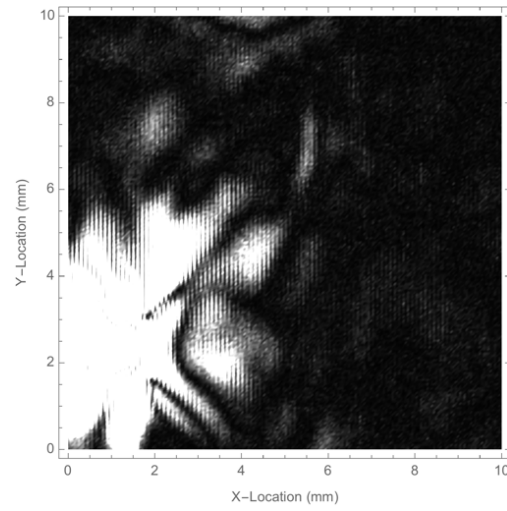


Figure 3.5(b) $t = 1.1 \mu\text{s}$

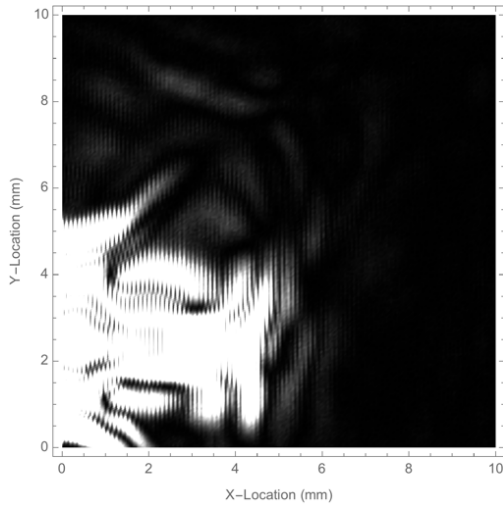


Figure 3.5 (c) $t = 1.2 \mu\text{s}$

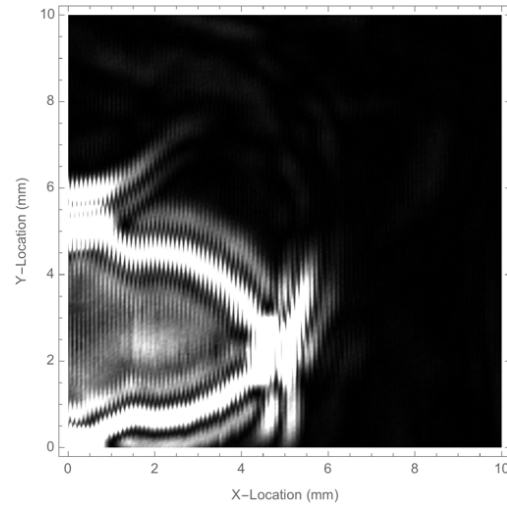


Figure 3.5 (d) $t = 1.3 \mu\text{s}$

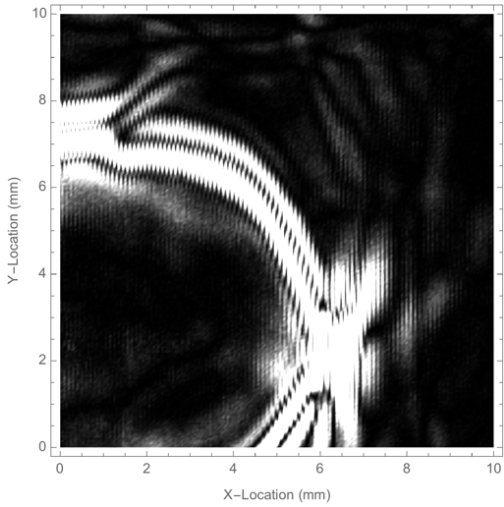


Figure 3.5 (e) $t = 1.4\mu\text{s}$

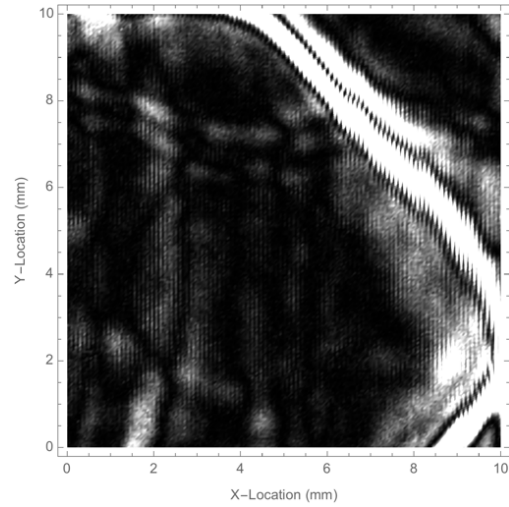


Figure 3.5 (f) $t = 1.6 \mu\text{s}$

3.3 Diffraction Pattern

To observe the internal diffraction effect mentioned in section 1.4, we use a tone burst signal at 9MHz and record a similar data cube as from last section to plot the flux diagram. Figure 3.6 shows the integrated flux on the same sample surface with an 18 cycle 9MHz tone burst signal integrating over $6\mu\text{s}$. Compared to the flux diagram above with the pulse signal, Figure 3.6 shows the expected effect of wavevector interference. There are intensity troughs and peaks both at the center of the sample and along the axis. However, the experiment data does not have the same resolution as the simulated data mentioned in previous chapter. One of the reasons is that, in order for the fringes to be well resolved, the excitation source needs to be coherent, i.e. a tone burst signal with a narrow bandwidth. Also, the transducers we are using has a measured focal spot size of 0.5mm, which limits the resolution of the observed pattern.

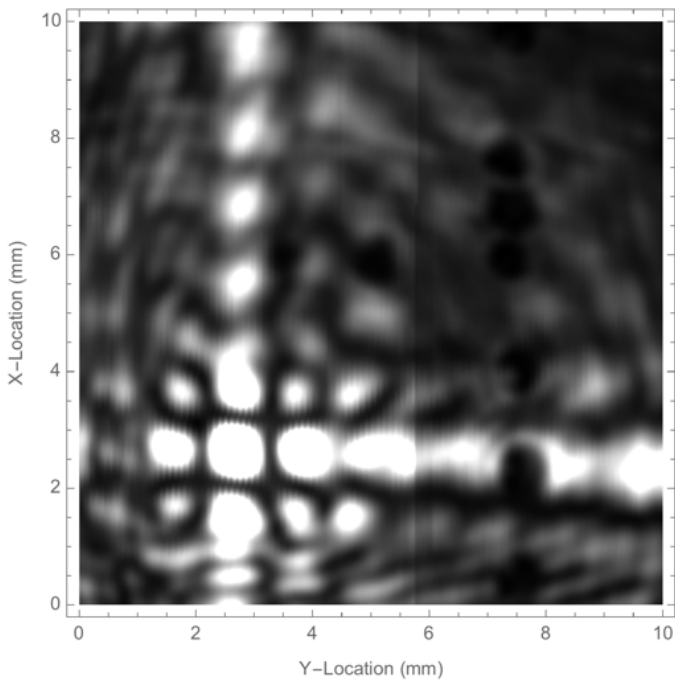


Figure 3.6 Diffraction pattern formed on Silicon surface from 9MHz 2 μ s Tone-Burst Signal

Another approach to observe the internal diffraction pattern is to Fourier transform the data cube and create single frequency flux diagrams. The Fourier transform changes the data cube from the original x-y-t into x-y- ω . This method requires a receiving transducer with a relatively wide bandwidth to record a spectrum of frequencies. Observing the intensity of a particular frequency component is equivalent to having a signal of the same length with narrowband frequency, which is perfect for increasing the resolution of the flux diagram. In Figure s 3.7 and 3.8 shown below, the Fourier transform of both the pulse and tone-burst signal shows the diffraction pattern. The pulse signal, when presented previously in Figure 3.4, has a wide bandwidth that we could not see any diffraction pattern. When we extract the higher frequency components “hidden” within the data, we can also observe the pattern. The higher the frequency of the component we extract, the finer the structure reflected in the flux diagram. The angle between maximum and minimum intensity is proportional to $\lambda^{2/3}$,

as shown on page 9, so interference at higher frequency will have shorter distances between maximum intensity points. The higher frequency components also have weaker intensity in general, since the pulse signal has prominent frequency at 9MHz.

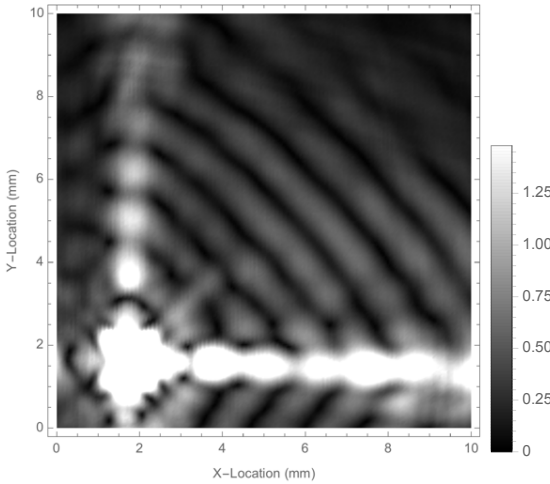


Figure 3.7 (a) Fourier transform of pulse signal at $f = 10$ MHz

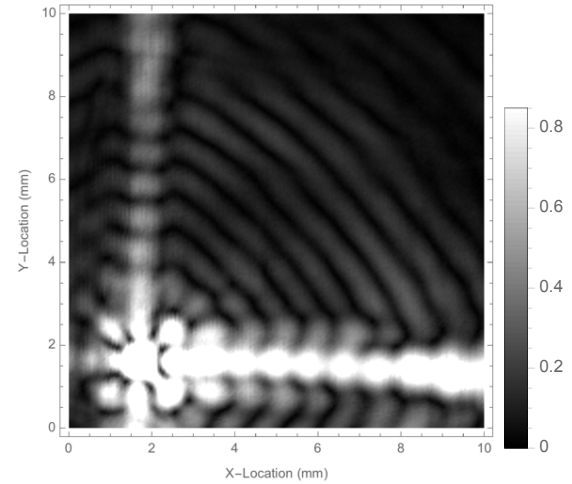


Figure 3.7 (b) Fourier transform of pulse signal at $f = 15$ MHz

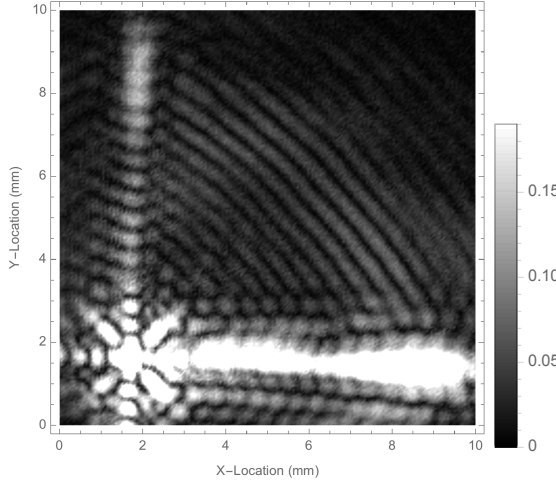


Figure 3.7 (c) Fourier transform of pulse signal at $f = 25$ MHz

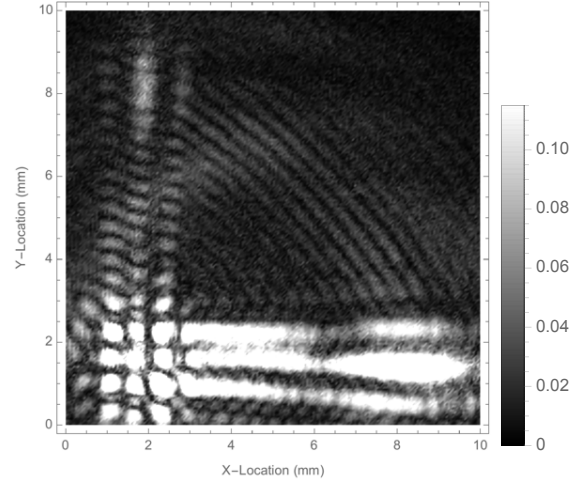


Figure 3.7 (d) Fourier transform of pulse signal at $f = 30$ MHz

The tone burst signal offers even finer diffraction structures, because of the longer signal length that allows more wavevectors to interfere with each others. We can observe this difference by comparing the diffraction pattern with two different signal lengths at the same frequency, for example, 25MHz, shown in 3.7 (c) and 3.8 (c). The tone-burst signal's flux diagrams also shows irregularity in the pattern. One possible

reason for the irregularity is that the tone burst signal is long enough to allow wavevectors from different modes to interfere. It will then create a different diffraction pattern from that expected interference of just two wavevectors from the slow transverse mode, as mentioned in section 1.4. If we compare the high intensity regions at different frequencies for the tone burst signal, we can see that frequencies that are multiples of 9MHz are stronger and show clearer diffraction patterns. For example, although 25 MHz is closer to the prominent 9 MHz than 27 MHz, Figure 3.8(c) has weaker intensity and murkier pattern than 3.8(d). This is because frequencies that are multiples of 9 MHz fit better in the signal time frame, which is determined by the number of cycles for 9MHz waves.

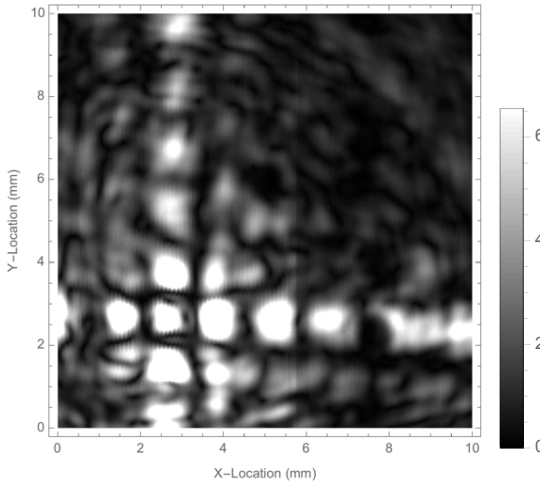


Figure 3.8 (a) Fourier transform of tone-burst signal at $f = 17$ MHz

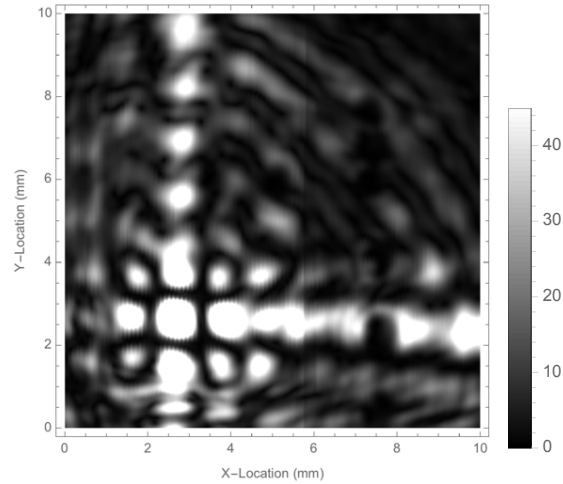


Figure 3.8 (b) Fourier transform of tone-burst signal at $f = 18$ MHz

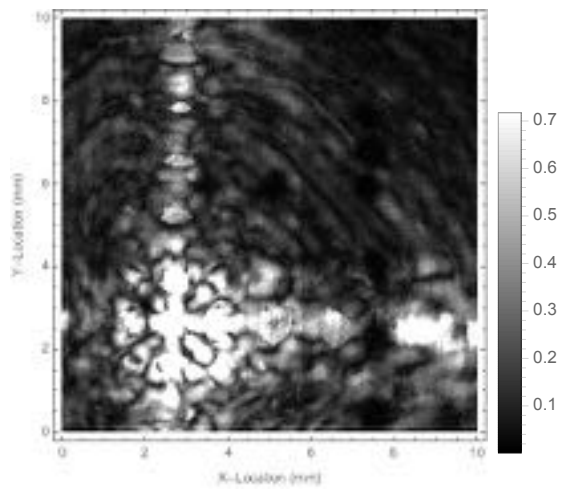


Figure 3.8 (c) Fourier transform of tone-burst signal at $f = 25$ MHz

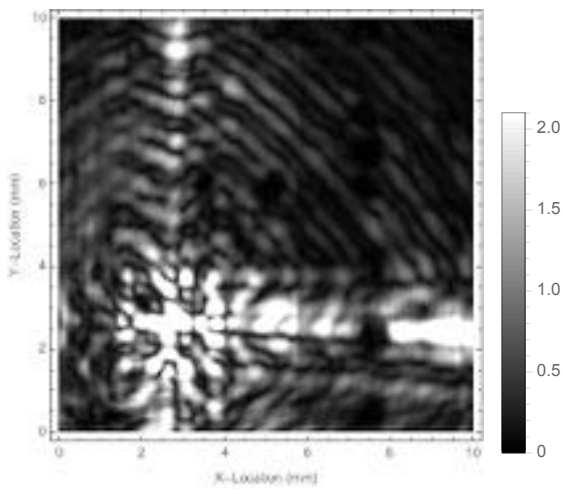


Figure 3.8 (d) Fourier transform of tone-burst signal at $f = 27$ MHz

Conclusion

Solving the elastic wave equation, we can construct the slowness surface for silicon. The inflection points on the slowness surface cause concentrations of group velocities in certain directions. As a result, the energy propagates anisotropically.

Experimentally observing both the arrival of wavefronts at a given location and the overall energy intensity on the surface shows the anisotropic propagation in silicon, as predicted by theory.

For observing diffraction patterns, using Fourier transform can not only isolate frequency components to reveal patterns previously unable to see, it also offers an alternative to actively control the signal source.

For future work, if we can obtain a waveform generator that generates pulse or tone burst signals at higher frequencies, we can also compare the effect of bandwidth on the diffraction pattern. The signal generated by the waveform generator has a relatively wide bandwidth, while the Fourier transform data is equivalent to a narrow-band signal.

Another potential direction to expand this project is to apply both the theoretical analysis and experiments on other anisotropic crystals.

References

- [1] Every, A. G., Wolfgang Sachse, K. Y. Kim, and M. O. Thompson. 1990. "Phonon Focusing and Mode-Conversion Effects in Silicon at Ultrasonic Frequencies." *Physical Review Letters* 65 (12): 1446-1449.
- [2] Hauser, Matt R., R. L. Weaver, and J. P. Wolfe. 1992. "Internal Diffraction of Ultrasound in Crystals: Phonon Focusing at Long Wavelength." *Physical Review Letters* 68 (17): 2604-2607.
- [3] Hauser, Matt Russell. 1995. *Acoustic Waves in Crystals*. PhD Thesis, Urbana, Illinois: University of Illinois at Urbana-Champaign.
- [4] Pluta, M., A.G. Every, W. Grill, and T.J. Kim. 2003. "Fourier inversion of acoustic wave fields in anisotropic solids." *Physical Review B* 67: 67-094117.
- [5] Wolfe, James P. 1998. *Imaging Phonons*. New York, NY: Cambridge University Press.

Appendix

Color Images in Black and White

